Modelling and Nanoscale Force Spectroscopy of Frequency Modulation Atomic Force Microscopy

Amir Farokh Payam

School of Engineering, Ulster University, Belfast, UK.

a.farokh-payam@ulster.ac.uk

Abstract— **In this paper, a simulation model for frequency modulation atomic force microscopy (FM-AFM) operating in constant amplitude dynamic mode is presented. The model is based on the slow time varying function theory. The mathematical principles to derive the dynamical equations for the amplitude and phase of the FM-AFM cantilever-tip motion is explained and the stability and performance of its closed-loop controller to keep the amplitude at constant value and phase at 90º is analysed. Then, the performance of the theoretical model is supported by comparison of numerical simulations and experiments. Furthermore, the transient behaviour of amplitude, phase and frequency shift of FM-AFM is investigated and the effect of controller gains on the transient motion is analysed. Finally, the derived FM-AFM model is used to simulate the single molecule/nanoscale force spectroscopy and study the effect of sample viscosity, stiffness and Hamaker constant on the response of FM-AFM.**

***Keywords*— Slow time varying function; amplitude; phase; frequency modulation AFM; dissipation; virial**

I. INTRODUCTION

Since its invention [1], atomic force microscope (AFM) demonstrates outstanding opportunities for imaging, characterization and manipulation of a wide variety of surfaces such as DNA, proteins, semiconductors, metals, polymers and composites at nanoscale with high spatial and true atomic resolution in ambient environments [2]-[10]. Between several configurations of AFM techniques, dynamic AFM remains the most widely used approach for imaging and characterization of nano materials [9]. The major advantages of dynamic AFM in comparison with contact mode are: (i) the presence of various parameters (amplitude, frequency, phase shift and cantilever deflection) sensitive to the interaction between tip and sample; (ii) decrease of lateral force during imaging; (iii) potential to image soft matter by inserting small force; (iv) low risk of damaging the samples and the tip and (v) obtaining images with atomic resolution of reactive surface at ultra-high vacuum (UHV) [11].

Frequency modulation atomic force microscopy (FM-AFM) has a significant ability of imaging surface topography of samples on an atomic scale especially with the vast applications as non-contact atomic force microscopy in ultra-high vacuum [11]-[13]. Analysis of the FM-AFM shows complicated relationship between the parameters of probe dynamics and the interaction force [11], [14]-[18]. In FM-AFM, the detection of resonance frequency variations of oscillating cantilever due to the interaction with the sample is used in the feedback loop to ensure that the phase shift between cantilever tip signal and drive signal is 90º. It means that the cantilever always oscillated at its resonance frequency. In FM-AFM the Phase-Locked loop is used to provide the feedback signal. Besides that, the cantilever oscillation amplitude is kept constant by an automatic gain controller (AGC) [19]-[23]. To achieve high resolution images, accurate quantification of experimental data, remove artefacts from images, reduce the effect of noise and avoid damage to the tip or sample during scanning, proper adjustment of control feedback parameters is essential [24]-[28]. Generally, choosing low gains for the feedback loop may be led to parachuting effect. This means when the height changes significantly, the tip cannot follow the surface accurately and some features of the surface will be lost during scanning [25]. On other hand, if the gains are set at high values, the overshoot of set-point is happened which leads to the ringing of cantilever during scanning the sample which affect the quality and resolution of images. In [24], a methodology to determine stable feedback gains based on the cantilever parameters and environment of imaging for FM-AFM is presented. This analysis and implementation has been performed for the steady state operation of FM-AFM.

One of the main advantages of FM-AFM is the decoupling of conservative and non-conservative forces. The conservative forces are related to the shift of frequency while the drive amplitude of AGC is proportional to the dissipative interaction between tip and sample [16]-[17], [29]-[30]. Several theoretical models and analysis have been developed to describe the FM-AFM behaviour [19]-[21], [31]-[35]. All of the methods have been used for the simulation and modelling of FM-AFM are concentrated on the development of PLL system. A PLL is used to demodulate the interaction forces between tip and sample from motion of cantilever. The demodulated signal is used as the feedback signal and can be used to generate both topography and dissipation images. However, in the simulation of FM-AFM using PLL system, it is necessary to solve FM-AFM equations numerically and a proper design of PLL is vital for FM-AFM performance which makes the FM-AFM simulation complex [19], [31]-[32]. Also, there is no direct access to the phase signal, and phase should be extracted by PLL from cantilever motion signal. So, for the analysis of the transient motion and simulation of FM-AFM behaviour, the alternative mathematical method for control system is preferred. In this paper, based on the slow time varying function theory [36]-[40], the dynamical equations for the amplitude and phase of AFM is derived and by adding control system to keep the phase at 90º and amplitude of cantilever oscillation at fixed value, the FM-AFM is modelled. The most advantages of the proposed dynamical model are not only independency of modelling and simulation to the PLL system but also the direct access to the amplitude and phase signals and capability of investigating the transient behaviour of phase and amplitude beside their steady state motion. The study of the amplitude, frequency and phase response in transient regime can be led to the increase of speed and precision of feedback control which has direct influence of the image precision [40]-[45]. This opens the possibility to capture the information conveyed by the sensing tip in a transient motion of cantilever, contrasted to the steady state used in current dynamic techniques [45]. The presented approach provides the opportunity to study the effect of feedback gains on the transient response of cantilever in FM-AFM. To validate the accuracy of the proposed model, the performance of the closed loop control system is analysed, and its stability is proved. The single molecule/nanoscale spectroscopy with FM-AFM is numerically simulated and compared with available experimental results [46]. Comparison shows very good agreement between simulated and experimental results which confirm the validity of the proposed model. Then, using the proposed model, the effect of sample viscosity, stiffness and Hamaker constant on the response of FM-AFM behaviour is investigated.

II. DYNAMICS EQUATION OF FM-AFM

In dynamic AFM, the cantilever-tip motion is approximately described by [39]:

$$\ddot{z}+\frac{\omega_0}{Q}\dot{z}+\omega_0^2 z=\frac{\omega_0^2 F_{ts}}{k}+\frac{\omega_0^2 F_d}{k} \tag{1}$$

Where ω_0, k and $Q$are resonance frequency, spring constant and quality factor of cantilever, respectively. F_{ts} is the interaction force between tip and sample and the drive force is described by:

$$F_d = F_{exc}\cos(\omega t) \tag{2}$$

Where F_{exc} is the excitation signal which can be determined by the controller to keep the amplitude of the cantilever at fixed value.

Assume that the solution of equation (1) is represented as:

$$z = A\cos(\omega t-\phi) \tag{3}$$

Where the amplitude A and the phase ϕ are slowly varying functions of time. Based on slow varying function theory and by defining $\beta=\omega t-\phi$ and $\sigma=\omega^2-\omega_0^2$ where ω_0 is the resonance frequency of cantilever when there is no interaction between tip and sample and ω is its resonance frequency when the interaction between tip and sample is occurred, the dynamic equations of amplitude and phase are derived as [40]:

$$\dot{A}=\frac{A\sin(2\beta)}{2\omega}\sigma-\frac{\omega_0^2}{\omega k}\sin(\beta)\left(F_{ts}+F_{exc}\cos(\omega t)\right)-\frac{A\omega_0}{2Q}\left(1-\cos(2\beta)\right) \tag{4}$$

$$\dot{\phi}=\frac{\cos^2(\beta)}{\omega}\sigma+\frac{\omega_0^2}{A\omega k}\cos(\beta)\left(F_{ts}+F_{exc}\cos(\omega t)\right)+\frac{\omega_0}{2Q}\sin(2\beta) \tag{5}$$

Based on equations (4)-(5), the dynamics equations of amplitude and phase are obtained. In the constant amplitude FM-AFM in addition of distance controller, there are two control schemes to keep the amplitude at fixed value and maintain the oscillation of cantilever at its resonance frequency (Fig.1).

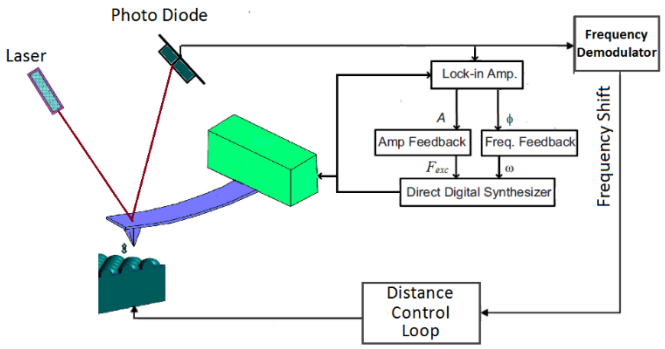

Figure 1. Schematic representation of FM-AFM.

In the first control scheme, a frequency feedback loop is used to keep the phase shift between the motion signal of cantilever and drive signal 90°. It means that in this situation, the cantilever is oscillated at its resonance frequency independent of any tip-sample interaction [24]. In the second scheme, the amplitude of cantilever is maintained at constant value.

In FM-AFM, as shown in Fig.1, the mentioned regulators operate independently from distance regulator. To model the controllers following equations are designed:

$$F_{exc} = -K_1 A - K_2 W_1 \tag{6}$$

$$\dot{W}_1 = A - A_{sp} \tag{7}$$

$$\sigma = -K_3 \phi - K_4 W_2 \tag{8}$$

$$\dot{W}_2 = \phi - \phi_{sp} \tag{9}$$

Where A_{sp} is the amplitude set-point, $\phi_{sp} = \pi / 2$ and $K_1 - K_4$ are gain parameters. It is clear that the FM-AFM is modelled without direct modelling of PLL, which makes the proposed model very simple and user friendly. Equations (4)-(9) can be used to simulate the FM-AFM behaviour.

To obtain fully transient dynamics equation of FM-AFM, equations (6)-(9) can be replaced in equations (4) and (5) and following expressions can be obtained:

$$\dot{A} = \frac{A\sin(2\beta)}{2\omega}(-K_3\phi - K_4 W_2) - \frac{\omega_0^2}{\omega k}\sin(\beta)\left(F_{ts} + (-K_1 A - K_2 W_1)\cos(\omega t)\right) - \frac{A\omega_0}{2Q}\left(1 - \cos(2\beta)\right) \tag{10}$$

$$\dot{\phi} = \frac{\cos^2(\beta)}{\omega}(-K_3\phi - K_4 W_2) + \frac{\omega_0^2}{A\omega k}\cos(\beta)\left(F_{ts} + (-K_1 A - K_2 W_1)\cos(\omega t)\right) + \frac{\omega_0}{2Q}\sin(2\beta) \tag{11}$$

$$\dot{W}_1 = A - A_{sp} \tag{12}$$

$$\dot{W}_2 = \phi - \phi_{sp} \tag{13}$$

Integrating equations (4) and (5) in a period of oscillation gives:

$$\dot{A} = -\frac{A\omega_0}{2Q} + \frac{F_{exc}\omega_0^2 \sin\phi}{2k\omega} - \frac{\omega_0^2}{2\pi k\omega^2}\int_0^{2\pi} F_{ts}\sin\beta d\beta \tag{14}$$

$$\dot{\phi} = \frac{\sigma}{2\omega} + \frac{F_{exc}\omega_0^2\cos\phi}{2Ak\omega} + \frac{\omega_0^2}{2A\pi k\omega^2}\int_0^{2\pi} F_{ts}\cos\beta d\beta \tag{15}$$

By considering the definition of energy dissipation and virial [47]-[48], the FM-AFM dynamics model is converted to:

$$\dot{A} = -\frac{A\omega_0}{2Q} + \frac{F_{exc}\omega_0^2\sin\phi}{2k\omega} - \frac{\omega_0^2}{2k\omega^2}e_{ts} \tag{16}$$

$$F_{exc} = -K_1 A - K_2 W_1 \tag{17}$$

$$\dot{W}_1 = A - A_{sp} \tag{18}$$

$$\dot{\phi} = \frac{\sigma}{2\omega} + \frac{F_{exc}\omega_0^2\cos\phi}{2Ak\omega} + \frac{\omega_0^2}{2Ak\omega^2}v_{ts} \tag{19}$$

$$\sigma = -K_3\phi - K_4 W_2 \tag{20}$$

$$\dot{W}_2 = \phi - \phi_{sp} \tag{21}$$

where e_{ts} is the energy dissipated during the tip-sample interaction and v_{ts} is the virial of the tip-sample interaction [47]-[48].

In the steady state we have:

$$\dot{A} = \dot{\phi} = \dot{W}_1 = \dot{W}_2 = 0 \tag{22}$$

So:

$$A = A_{sp} \tag{23}$$

$$\phi = \phi_{sp} = \pi / 2 \tag{24}$$

$$0 = -\frac{A_{sp}\omega_0}{2Q} - \frac{(K_1 A_{sp} + K_2 W_1)\omega_0^2}{2k\omega} - \frac{\omega_0^2}{2k\omega^2} e_{ts} \tag{25}$$

$$0 = -\frac{1}{2\omega}(K_3\phi_{sp} + K_4 W_2) + \frac{\omega_0^2}{2A_{sp}k\omega^2} v_{ts} \tag{26}$$

Hence:

$$W_{10} = -\frac{k\omega A_{sp}}{K_2\omega_0 Q} - \frac{K_1}{K_2} A_{sp} - \frac{e_{ts}}{\omega K_2} \tag{27}$$

$$W_{20} = \frac{K_3}{K_4}\frac{\pi}{2} - \frac{\omega_0^2}{A_{sp}k\omega K_4} v_{ts} \tag{28}$$

To analyse the closed loop response of the controller, both frequency and amplitude loops should be active, while one setpoint is modulated the other remains constant [24].

In order to examine the stability of the amplitude controller in the steady state motion, small perturbations ΔA, ΔW_1 are introduced:

$$A = A_{sp} + \Delta A \tag{29}$$

$$W_1 = W_{10} + \Delta W_1 \tag{30}$$

Substituting equations (29)-(30) into expressions (16)-(21), the following equations are obtained (mathematical details are given in Appendix):

$$\begin{bmatrix} \Delta\dot{A} \\ \Delta\dot{W}_1 \end{bmatrix} = \begin{bmatrix} -\left(\frac{\omega_0}{2Q} + \frac{K_1\omega_0^2}{2k\omega}\right) & -\frac{K_2\omega_0^2}{2k\omega} \\ 1 & 0 \end{bmatrix} \begin{bmatrix} \Delta A \\ \Delta W_1 \end{bmatrix} \tag{31}$$

The characteristic equations of (31) is:

$$\lambda^2 + \lambda\left(\frac{\omega_0}{Q} + \frac{K_1}{k\omega}\right) + \frac{K_2}{k\omega} = 0 \tag{32}$$

Hence, the sufficient conditions for the stability of the controller to keep the amplitude at constant value are:

$$K_1 > 0,\ K_2 > 0, \tag{33}$$

It is in agreements with the fact that a controller for a minimum phase system cannot have negative PI gains.

However, because choosing high values for the gains maybe led to the amplifying of the noise and vibration in the amplitude or phase signals, practically it is not possible to choose high positive values for the gains. Also, if the gain values are chosen very high, due to the imposed vibration in the amplitude and/or phase signals, the controller cannot be converged. It will be discussed more with the simulation results.

Similarly, to examine the stability of the phase controller in the steady state motion, small perturbations $\Delta\phi$, ΔW_2 are introduced:

$$\phi = \phi_{sp} + \Delta\phi \tag{34}$$

$$W_2 = W_{20} + \Delta W_2 \tag{35}$$

Substituting equations (34)-(35) into expressions (16)-(21), the following equations are obtained (mathematical details are given in Appendix):

$$\begin{bmatrix} \Delta\dot{\phi} \\ \Delta\dot{W}_2 \end{bmatrix} = \begin{bmatrix} -\frac{K_3}{2\omega} - \frac{\omega_0}{2Q} - \frac{\omega_0^2 e_{ts}}{2k\omega^2} & -\frac{K_4}{2\omega} \\ 1 & 0 \end{bmatrix} \begin{bmatrix} \Delta\phi \\ \Delta W_2 \end{bmatrix} \tag{36}$$

The characteristic equation of (36) is:

$$\lambda^2 + \lambda\left(\frac{K_3}{2\omega} + \frac{\omega_0}{2Q} + \frac{\omega_0^2 e_{ts}}{2\pi k\omega^2}\right) + \frac{K_4}{2\omega} = 0 \tag{37}$$

Again, the sufficient conditions for the stability are

$$K_3 > 0,\ K_4 > 0 \tag{38}$$

Here also to have convergence in the control system and accurate simulation, the values of the gains cannot be chosen very high.

III. Results and Discussion

In order to simulate the FM-AFM behaviour, it is necessary to model the interaction force between cantilever-tip system and sample. The interaction force can be described by conservative and non-conservative viscoelastic forces by the following models [40]:

$$F_{tsc} = \begin{cases} -\dfrac{HR}{6d^2} & d \geq a_0 \\ -\dfrac{HR}{6a_0^2} + \dfrac{4E_{eff}\sqrt{R}}{3}(a_0 - d)^{3/2} & d < a_0 \end{cases} \quad \text{(39-a)}$$

$$F_{tsnc} = \begin{cases} 0 & d \geq a_0 \\ -\eta\sqrt{R(a_0 - d)}\dot{d} & d < a_0 \end{cases} \quad \text{(39-b)}$$

Where H is the Hamaker constant, $E_{eff} = \left[(1-\nu_s^2)/E_s + (1-\nu_t^2)/E_t\right]^{-1}$ is the effective Young Modulus of the interaction, E_t, E_s, ν_t and ν_s are Young Moduli and Poisson's ratios of tip and sample, respectively. R is the tip radius and η is the viscosity of the sample. In this paper, for simulations the tip was characterized by $E_{tip} = 160\ GPA$ and $\nu_t = 0.45$.

The numerical simulation of equations (4)-(9) was calculated by a fourth-order Runge-Kutta algorithm in C++ software. Note that the simulations have been performed based on the normalized time ($\tau = \omega_0 t$).

First, to evaluate the validity of the proposed model, especially for the simulation of single molecule/nanoscale force spectroscopy, the experiment [46] which performed on the single PTCDA on the Si(111)-(7× 7) surface is reproduced by numerical simulation based on the proposed model for FM-AFM. The frequency shift curves measured over the center of PCTDA molecules, corner adatoms and corner holes are shown in Fig.5-b [46]. The parameters of cantilever of the experiment which is used in numerical simulation are $k = 29.6\frac{N}{m}, Q = 25000, f_0 = 156.719\ kHz, A = 20.1\ nm\ and\ R = 4.35$nm. For the PTCDA, the simulation parameters are $H = 6.85 \times 10^{-19}\ J, E = 4.36\ GPa, a_0 = 0.73\ nm$. For Corner adatom, $H = 5.85 \times 10^{-19}\ J, E = 1.5\ GPa, a_0 = 0.64\ nm$ and corner hole $H = 5.85 \times 10^{-19}\ J$. The controller gains are selected as $K_1 = 7 \times 10^{-8}, K_2 = 10^{-5}, K_3 = 0.2$ and $K_4 = 6.5$.

The Numerical simulations of PTCDA, corner adatom and corner hole are given in Fig.2-a. Comparison between Figs.2-a and b shows very good agreement between numerical simulation and experiment [46] with the error less than 5% which proves the validity and high accuracy of the proposed model of FM-AFM especially for the simulation of the single molecule/nanoscale force spectroscopy.

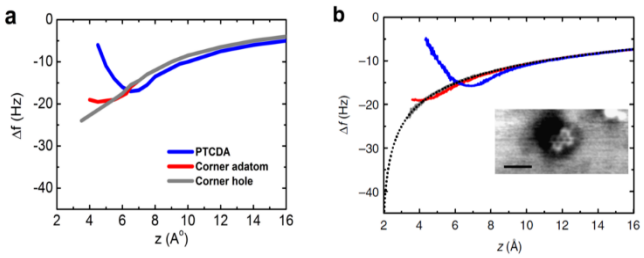

Figure 2. Comparison between numerical simulation (a) and experiment [46] (b) of molecule spectroscopy using FM-AFM for PTCDA molecule on the Si(111)-(7× 7), Creative Commons CC BY License.

In order to analyze the FM-AFM behavior, investigate the effect of feedback controller gains on the transient response of FM-AFM and effect of conservative and dissipative interaction between tip and sample, several numerical simulations have been carried out. In the simulations the cantilever parameters for FM-AFM are considered as $k = 4\ \frac{N}{m}, Q = 240, f_0 = 156.719\ kHz$ and $R = 3\ nm$. The gains of controller keep the same in all of the simulations.

In Fig.3-a, the frequency shift versus distance curve is shown. This curve is obtained by numerical calculation of equations (4)-(9) for various average distance. As it is demonstrated, in the attractive regime, the frequency shift has negative value which means the resonance frequency of cantilever decreases. In contrast, when there is a repulsive interaction between cantilever-tip and sample, the frequency shift has a positive value which describes increase in the resonance frequency. Figs.3-b,c,d show the amplitude, phase and frequency shift versus time, when the cantilever is far from the sample, in attractive regime and in repulsive regime, respectively. As it is shown, based on the presented simulation model, the transient behaviour of amplitude, phase and frequency shift can be obtained. In contrast of transient behaviour of AM-AFM [40], which the interaction regime between tip and sample significantly influence the transient motion of cantilever-tip signal, in FM-AFM the role of controllers to keep the amplitude and phase at constant values is significant. In other words, while as shown in Figs. 4-5 of [40] in AM-AFM there is a significant differences in the transient behaviour of amplitude and especially phase in attractive regime in comparison with repulsive regime, in FM-AFM there is not significant differences in transient response of amplitude and phase between attractive and repulsive regimes which is attributed to the role of controller in FM-AFM which keep the amplitude at fixed value and phase at 90° in steady state. It demonstrates in FM-AFM, as the figures 3-b and c show, the transient behaviour of amplitude and phase are dependent on the controller gains. However, the transient response of frequency shift before it reaches to its steady state value can be explained by the interaction regime. As it can be seen from amplitude signal (Fig. 3-b), before it reaches to its constant value (here is 10 (nm)), it has higher value than 10 (nm) which means depend on the average distance between cantilever and sample surface, it can be in repulsive or attractive regime of interaction. In the Fig. 3-d, when the cantilever is far from sample ($\sim 5 - 25\ nm$), in the transient part, it goes to the weak attractive regime, which means there is a negative frequency shift at transient part which can be seen from figure 3-d. In other hand, when the cantilever is in the intermittent contact with the sample, in the transient motion, there is a positive shift in the frequency of the cantilever which its peak is attributed to the maximum transient amplitude and by approaching the transient amplitude toward the steady state value, the transient frequency shift also decreases toward its steady state response. However, from transient response, it is clearly obvious that in the intermittent contact regime, there is a positive shift in the frequency of the cantilever.

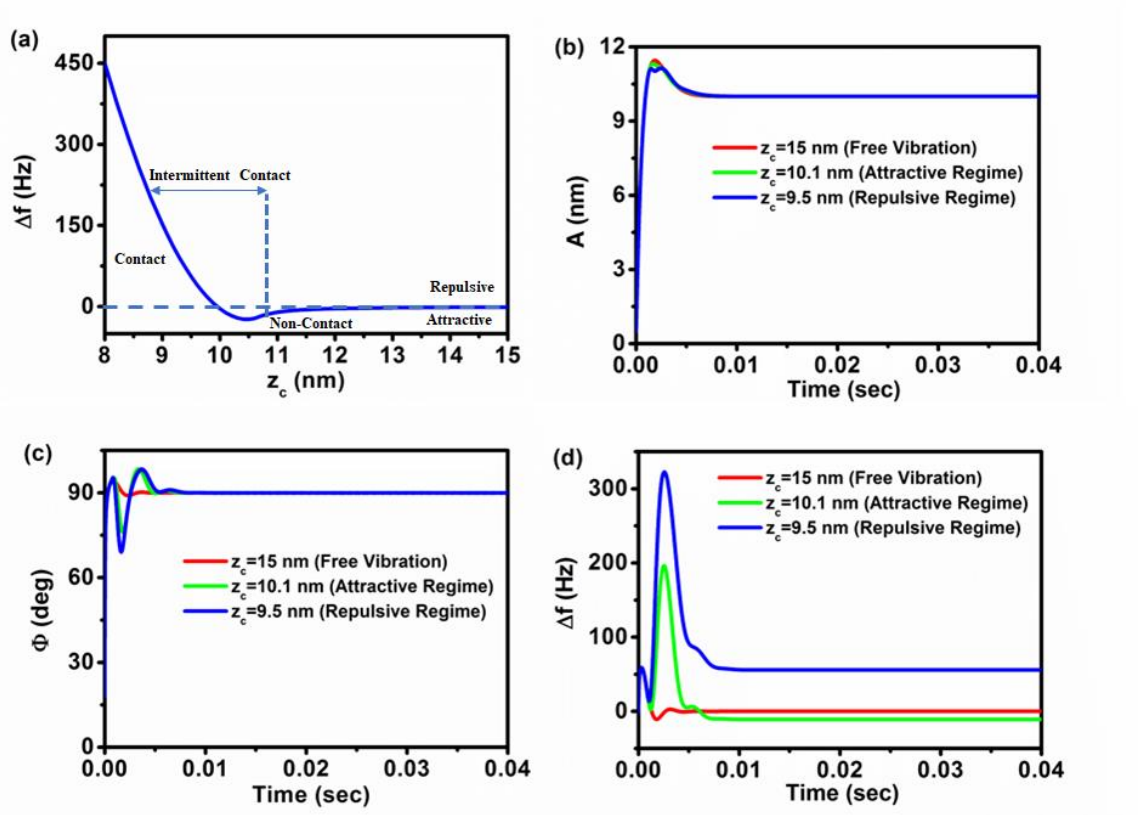

Figure 3. a) Frequency shift versus average distance, transient and steady state response of b) amplitude, c) phase and d) frequency shift of cantilever. The simulation parameters are: $R = 3\ (nm), k = 4\frac{N}{m}, Q = 240, H = 5 \times 10^{-20}(J), E_{eff} = 100\ MPa, E_s = 85\ MPa, v_s = 0.4,$ $A = 10\ (nm), a_0 = 0.164nm.$

In order to investigate the effect of controller gain values on the transient and steady state response of frequency shift and stability of cantilever, another simulation has been carried out. As the results of Fig. 4 shows, there is a trade-off between gain values, transient time and stability. Based on the results, if the gains are too low, the transient time is longer and increasing the gains leads to the decrease of transient time. In other words, increasing the gains values generates more noise and vibration in the transient part of cantilever and if the values of gains will be too high, it leads to instability of cantilever and steady state behaviour will not be achieved.

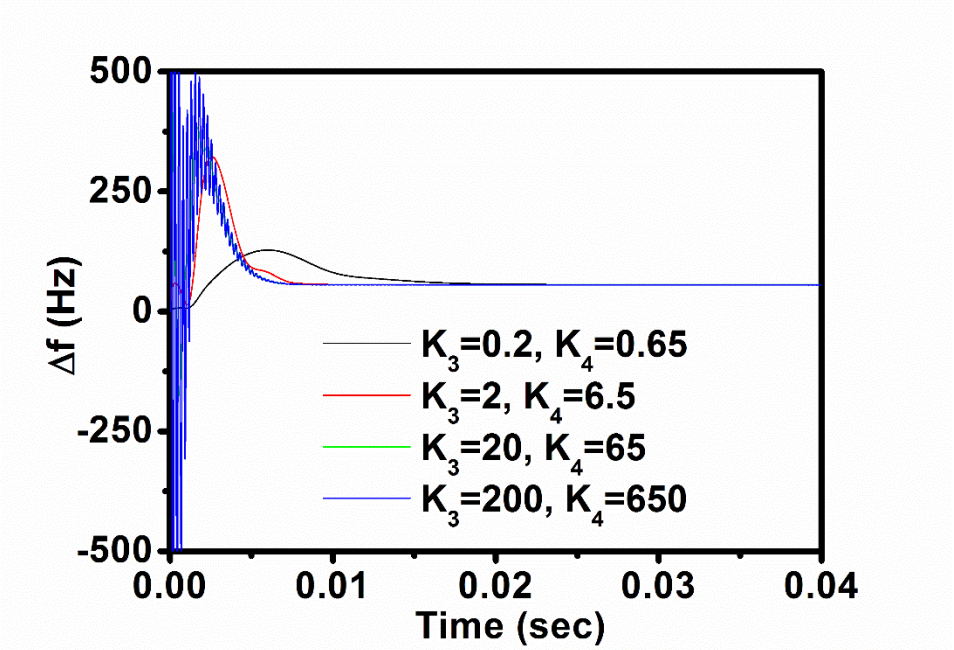

Figure 4. Transient and steady state behaviour of frequency shift for different controller gains. The simulation parameters are: $R = 3\ (nm), k = 4\frac{N}{m}, Q = 240, H = 5 \times 10^{-20}(J), E = 100\ MPa, A = 10\ (nm)$ and $z_c = 9.5\ (nm)$, $f_0 = 156.719\ kHz$.

Figure 5 shows the frequency shift of FM-AFM versus distance for different stiffness and Hamaker constant with same viscosity as $\eta = 100\ Pa.s$. As the results show, for the case that the samples have similar stiffness but different Hamaker constant, increasing Hamaker constant leads to the increase of frequency shift in attractive regime (decrease of resonance frequency). This is becauseof the role of Hamaker constant in increase of the attractive force of the tip-sample interaction which reduces the resonance frequency of cantilever [49]. In other hand, in the case of the same Hamaker constant and different stiffness, for the same indentation, the higher stiff material makes higher shift in the frequency (increase the resonance frequency). Also, it is obvious that the AFM tip can indent more in the softer sample.

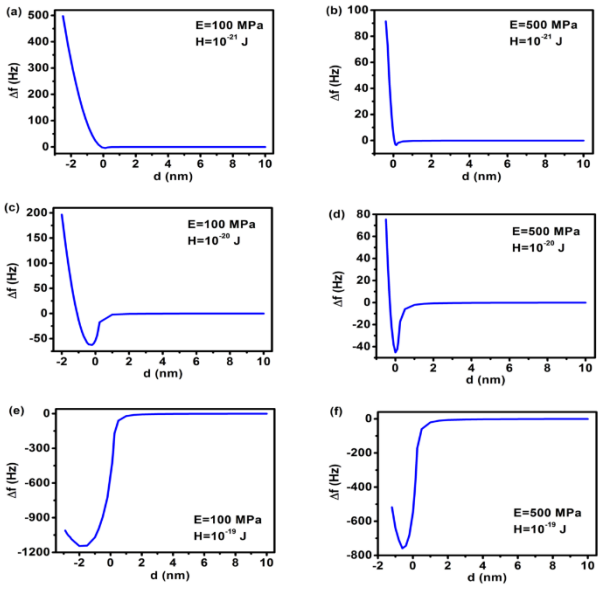

Figure 5. Frequency response of FM-AFM for different samples with different stiffness and Hamaker constant.

In order to evaluate the effect of dissipation on the excitation force, by adding different viscosities to the interaction force, the FM-AFM behaviour is simulated. The results are given in Fig.6. As it can be seen, for the case of same viscosity and different stiffness and Hamaker constant (Figs. 6-a, c, and e and Figs. 6-b, d and f), while the values of Young-modulus and Hamaker constants are different, because there is not any change in viscosity, the excitation force for the same indentation length is the same. On the other hand, comparison between Figs.6-a and b, Figs.6-c and d and Figs.6-e and f, demonstrate that although the stiffness and Hamaker constant are same, due to changes of viscosity, the excitation force is changed. It means in FM-AFM variations of excitation force is directly related to the change of dissipation without any effect from conservative forces. The results show decoupling between conservative and dissipative forces in FM-AFM. Also it is depicted, when the viscosity of sample is increased, the excitation force will be increased.

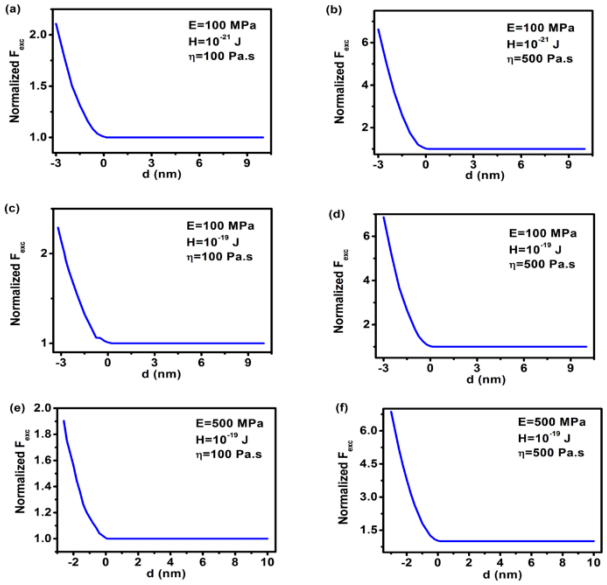

Figure 6. Normalized excitation force of FM-AFM for different samples with different stiffness, Hamaker constant and viscosity.

In order to analyze the imaging behavior, other simulations have been performed. In this case, the effect of topography variations, change of stiffness and Hamaker constant on the frequency shift of FM-AFM while scanning the surface of the sample is studied. It is depicted from the results of Fig.7 that in the case of the change in topography, if there is a contact between tip and sample, decreasing the average distance between tip and sample

leads to the increase of indentation (can be obtained from $Z_c - A$) and the resonance frequency is increased. Increasing the sample stiffness or decreasing the Hamaker constant also leads to the increase of resonance frequency. On the other hand, for the same topography and Hamaker constant, decreasing the stiffness leads to the decrease of resonance frequency.

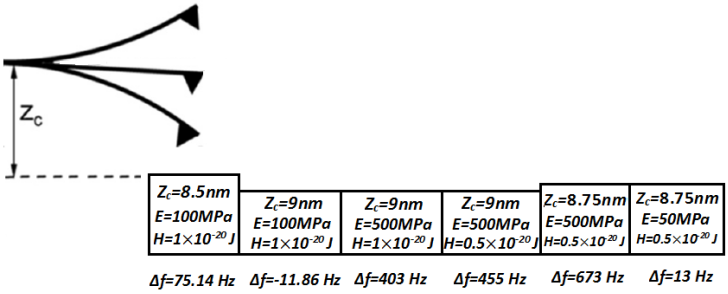

Figure 7. Normalized excitation force of FM-AFM for different samples with different stiffness and Hamaker constant. The viscosity of this simulation is $\eta = 100\ Pa.s$.

IV. Conclusion

In this paper, based on the slow time varying function theory, a mathematical model for the frequency modulated atomic force microscopy (FM-AFM) is derived. According to the proposed methodology, the dynamics equation of amplitude and phase of the AFM cantilever is extracted. Then, by adding control system to keep the phase at 90° and amplitude of cantilever oscillation at fixed value, the FM-AFM is modelled. The stability of the closed-loop controller to keep the amplitude at constant value and phase at 90° is analysed. Comparison between numerical simulation and experiments show very good agreement between simulated and experimental results and supports the performance of the theoretical model. For numerical simulation, the Runge-Kutta algorithm is used to solve the derived equations of FM-AFM. Based on the numerical simulations the effects of sample viscosity, stiffness and Hamaker constant on the response of FM-AFM are investigated.

Acknowledgment

The author gratefully acknowledges Dr. Christian Dietz from Technische Universität Darmstadt for fruitful discussion.

Appendix

Following equations are the dynamics equations governing the FM-AFM behaviour:

$$\dot{A} = -\frac{A\omega_0}{2Q} + \frac{F_{exc}\omega_0^2 \sin\phi}{2k\omega} - \frac{\omega_0^2}{2\pi k\omega^2} e_{ts} \tag{A1}$$

$$F_{exc} = -K_1 A - K_2 W_1 \tag{A2}$$

$$\dot{W}_1 = A - A_{sp} \tag{A3}$$

$$\dot{\phi} = \frac{\sigma}{2\omega} + \frac{F_{exc}\omega_0^2 \cos\phi}{2Ak\omega} + \frac{\omega_0^2}{2A\pi k\omega^2} v_{ts} \tag{A4}$$

$$\sigma = -K_3\phi - K_4 W_2 \tag{A5}$$

$$\dot{W}_2 = \phi - \phi_{sp} \tag{A6}$$

In the steady state:

$$\dot{A} = \dot{\phi} = \dot{W}_1 = \dot{W}_2 = 0 \tag{A7}$$

$$A = A_{sp} \tag{A8}$$

$$\phi = \phi_{sp} = \pi/2 \tag{A9}$$

Which leads to the following steady state equations:

$$0 = -\frac{A_{sp}\omega_0}{2Q} - \frac{K_1\omega_0^2}{2k\omega} A_{sp} - \frac{K_2\omega_0^2}{2k\omega} W_{10} - \frac{\omega_0^2}{2\pi k\omega^2} e_{ts} \tag{A10}$$

$$0=-\frac{K_3}{2\omega}\left(\phi_{sp}\right)\left(A_{sp}\right)-\frac{K_4}{2\omega}\left(W_{20}\right)\left(A_{sp}\right)+\frac{\omega_0^2}{2\pi k\omega^2}v_{ts} \quad \text{(A11)}$$

When small perturbations are introduced to the amplitude control loop, substituting equations (29)-(30) in (A1)-(A3) gives:

$$\Delta\dot{A}=-\frac{\omega_0}{2Q}\Delta A-\frac{\omega_0}{2Q}A_{sp}-\frac{K_1\omega_0^2}{2k\omega}A_{sp}-\frac{K_1\omega_0^2}{2k\omega}\Delta A-\frac{K_2\omega_0^2}{2k\omega}W_{10}-\frac{K_2\omega_0^2}{2k\omega}\Delta W_1-\frac{\omega_0^2}{2\pi k\omega^2}e_{ts} \quad \text{(A12)}$$

$$\Delta\dot{W}_1=\Delta A \quad \text{(A13)}$$

Considering the contribution of steady state equations (A10) in (A12) leads to the following expressions:

$$\Delta\dot{A}=-\frac{\Delta A\omega_0}{2Q}-\frac{K_1\omega_0^2}{2k\omega}\Delta A-\frac{K_2\omega_0^2}{2k\omega}\Delta W_1 \quad \text{(A14)}$$

When small perturbations are introduced to the frequency control loop, substituting equations (34)-(35) in (A4)-(A6) gives:

$$\Delta\dot{\phi}=-\frac{K_3}{2\omega}\left(\phi_{sp}+\Delta\phi\right)-\frac{K_4}{2\omega}\left(W_{20}+\Delta W_2\right)+\frac{\omega_0^2}{2kA_{sp}\omega}\left(K_1A_{sp}+K_2W_{10}\right)\Delta\phi+\frac{\omega_0^2}{2\pi kA_{sp}\omega^2}v_{ts} \quad \text{(A15)}$$

$$\Delta\dot{W}_2=\Delta\phi \quad \text{(A16)}$$

Considering the contribution of steady state equations (A11) in (A15) leads to the following expressions:

$$\Delta\dot{\phi}=-\frac{K_3}{2\omega}\Delta\phi-\frac{K_4}{2\omega}\Delta W_2+\frac{\omega_0^2}{2kA_{sp}\omega}\left(K_1A_{sp}+K_2W_{10}\right)\Delta\phi \quad \text{(A17)}$$

Substituting W_{10} from (23) in (A17) gives:

$$\Delta\dot{\phi}==-\left(\frac{K_3}{2\omega}+\frac{\omega_0}{2Q}+\frac{\omega_0^2e_{ts}}{2k\omega^2}\right)\Delta\phi-\frac{K_4}{2\omega}\Delta W_2 \quad \text{(A18)}$$

REFERENCES

[1] G. Binnig, C.F. Quate, Atomic Force Microscope, Phys. Rev. Lett. 56 (9) (1986) 930-933.

[2] H. Huang, et al. Local surface mechanical properties of PDMS-silica nanocomposite probed with intermodulation AFM, Compos. Sci. Technol. 150 (2017) 111-119.

[3] Y. F. Dufrene, et al. Imaging modes of atomic force microscopy for application in molecular and cell biology, Nat. Nanotechnol. 12 (2017) 295-307.

[4] K. Voïtchovsky, J.J. Kuna, S.A. Contera, E. Tosatti, F. Stellacci, Direct mapping of the solid-liquid adhesion energy with subnanometre resolution, Nat. Nanotechnol. 5 (6) (2010) 401-405.

[5] A.F. Payam, et al., Development of fatigue testing system for in-situ observation of stainless steel 316 by HS-AFM & SEM, Int. J. Fatigue 127 (2019) 1-9.

[6] G. Gramse, et al., Nondestructive imaging of atomically thin nanostructures buried in silicon, Sci. Adv. 3 (2017) 1-8.

[7] C. Barth, A.S. Foster, C.R. Henry, A.L. Shluger, Chemistry with high-resolution scanning force methods, Adv. Mater. 23 (2011) 477–501.

[8] M.R. Uhlig, D. Martin-Jimenez, R. Garcia, Atomic-scale mapping of hydrophobic layers on graphene and few-layer MoS2 and WSe2 in water, Nat. Commun. 10 (2019) 2606.

[9] R. Garcia, A. San Paulo, Attractive and repulsive tip-sample interaction regimes in tapping-mode atomic force microscopy, Phys. Rev. B 60 (1999) 4961-7.

[10] E.J. Miller, et al., Sub-nanometer Resolution Imaging with Amplitude-modulation Atomic Force Microscopy in Liquid, J. Vis. Exp. 118 (2016) e54924.

[11] R. Garcia, R. Perez, Dynamic atomic force microscopy methods, Surf. Sci. Rep. (2002) 47:197.

[12] F.J. Giessibl, Advances in atomic force microscopy, Rev. Mod. Phys. 75 (2003) 949.

[13] C. Barth, A. S. Foster, C. R. Henry, A. L. Shluger, Recent trends in surface characterization and chemistry with high-resolution scanning force methods, Adv. Mater. 23 (2011) 477.

[14] A. Labuda, Y. Miyahara, L. Cockins, P. H. Grutter, Decoupling conservative and dissipative forces in frequency modulation atomic force microscopy, Phys. Rev. B 84 (2011) 125433.

[15] K. Kuchuk, U. Sivan, Accurate, explicit formulae for higher harmonic force spectroscopy by frequency modulation-AFM, Beilstein J. Nanotechnol. 6 (2015) 149.

[16] J. E. Sader, S. P. Jarvis, Accurate formulas for interaction force and energy in frequency modulation force spectroscopy, Appl. Phys. Lett. 84 (2004) 1801.

[17] J. E. Sader, T. Uchihashi, M. J. Higgins, A. Farrell, Y. Nakayama, S. P. Jarvis, Quantitative force measurements using frequency modulation atomic force microscopy—theoretical foundations, Nanotechnol. 16, (2005) S94.

[18] A. F. Payam, M. Fathipour, Effect of tip mass on frequency response and sensitivity of AFM cantilever in liquid, Micron 70 (2015) 50-54.

[19] A. M. Bueno, J. M. Balthazar, J. R. C. Piqueira, Phase-Locked loops lock-in range in Frequency Modulated-Atomic Force Microscope nonlinear control system, Commun. Nonlinear. Sci. Numer. Simulat. 17 (2012) 3101.

[20] F. F. Canova, "*Simulating atomic processes in Non-contact Atomic Force Microscopy of ionic surfaces*," PhD Thesis, Department of Physics, Tampere University of Technology, Finland, 2012.

[21] F. J. Giessibl M. Tortonese, Self-oscillating mode for frequency modulation noncontact atomic force Microscopy, Appl. Phys. Lett. 70 (1997) 2590.

[22] S. Morita, R. Wiesendanger, E. Meyer, F.J. Giessibl, "*Noncontact atomic force microscopy*," Springer, Berlin, 2009.

[23] B. Bhushan, "*handbook of nanotechnology*," Springer, Berlin, 2004.

[24] J. I. Kilpatrick, A. Gannepalli, J. P. Cleveland, S. P. Jarvis, Frequency modulation atomic force microscopy in ambient environments utilizing robust feedback tuning, Rev. Sci. Instrum. 80 (2009) 023701.

[25] M.S. Skilbeck, "*Ultrasonics and Nanomechanics*," PhD Thesis, University of Warwick, 2017.
[26] J. Polesel-Maris, S. Gauthier, Noise in Frequency Modulation-Dynamic Force Microscopy, J. Phys.: Conf. Ser. 61 (2007) 949.
[27] B.I. Kim, Direct comparison between phase locked oscillator and direct resonance oscillator in the noncontact atomic force microscopy under ultrahigh vacuum, Rev. Sci. Instrum. 75 (2004) 5035.
[28] A.E. Gildemeister, T. Ihn, C. Barengo, P. Studerus, K. Ensslin, Construction of a dilution refrigerator cooled scanning force microscope, Rev. Sci. Instrum. 78 (2007) 013704.
[29] K. Suzuki, S. Kitamura, S. Tanaka, K. Kobayashi, H. Yamada, Development and Applications of a Frequency Modulation Atomic Force Microscope for High-resolution Imaging in Liquids, JEOL News 45 (2010) 24.
[30] F. J. Giessibl, S. Hembacher, M. Herz, C. Schiller, J. Mannhart, Stability considerations and implementation of cantilevers allowing dynamic force microscopy with optimal resolution: the qPlus sensor, Nanotechnol. 15 (2004) S79.
[31] L. Nony, A. Barato, D. Schaer, Ol. Pfeier, A. Wezel, et al., Non- contact atomic force microscopy simulator with phase-locked-loop controlled frequency detec- tion and excitation, Phys. Rev. B 74 (2006) 235439.
[32] A. M. Bueno, J.M. Balthazar, J.R. C. Piqueira, Simulations of the Frequency Modulated - Atomic Force Microscope (FM-AFM) Nonlinear Control System, Chaotic Model. Simulat. (CMSIM) 1 (2011) 173.
[33] C. Chawla, S. D. Solares, Single-cantilever dual-frequency-modulation atomic force microscopy, Meas. Sci. Technol. 20 (2008) 015501.
[34] G. Couturier, J. Aimé, J. Salardenne, R. Boisgard, A virtual non contact-atomic force microscope (nc-afm): simulation and comparison with analytical models, Eur. Phys. J. AP 15 (2001) 141.
[35] J. P. Maris, S. Gauthier, A virtual dynamic atomic force microscope for image calculations, J. Appl. Phys. 97 (2005) 044902.
[36] J. Melcher, D. M. Martin, M. Jaafar, J. G. Herrero, A. Raman, High-resolution dynamic atomic force microscopy in liquids with different feedback architectures, Beilstein J. Nanotechnol. 4 (2013) 153.
[37] A. Sinha, Nonlinear dynamics of atomic force microscope with PI feedback, J. Sound Vib. 288 (2005) 387.
[38] L. Nony, R. Boisgard, J. P. Aime, Nonlinear dynamical properties of an oscillating tip–cantilever system in the tapping mode, J. Chem. Phys. 111 (1999)1615.
[39] A.F. Payam, D.M. Jimenez, R. Garcia, Force Reconstruction from tapping mode force microscopy experiments, Nanotechnol. 26 (2015) 185706.
[40] A. F. Payam, Dynamic modeling and sensitivity analysis of dAFM in the transient and steady state motions, Ultramicroscopy 169 (2016) 55.
[41] D.R. Sahoo, "Transient force atomic force microscopy: systems approaches to emerging applications," PhD Thesis, Iowa State University, 2006.
[42] D.R. Sahoo, A. Sebastian, M.V. Salapaka, Transient-signal-based sample-detection in atomic force microscopy Appl. Phys. Lett. 83 (26) (2003) 5521-5523.
[43] D.R. Sahoo, A. Sebastian, M.V. Salapaka, Harnessing the transient signals in atomic force microscopy, Int. J. Robust Nonlinear Control 15 (2005) 805-820.
[44] S. Santos, K. Gadelrab, J. Font, M. Chiesa, Single-cycle atomic force microscope force reconstruction: resolving time-dependent interactions, New J. Phys. 15 (2013) 083034.
[45] E.A. López-Guerra, F. Banfi, S.D. Solares, G. Ferrini, Theory of Single-Impact Atomic Force Spectroscopy in liquids with material contrast, Sci. Rep. 8 (2018) 7534.
[46] K. Iwata, S. Yamazaki, P. Mutombo, P. Hapala, M. Ondracek, P. Jelinek, Y. Sugimoto, Chemical structure imaging of a single molecule by atomic force microscopy at room temperature, Nature Commun 6 (2015) 7766.
[47] A. San Paulo, R. García, Tip-surface forces, amplitude, and energy dissipation in amplitude-modulation (tapping mode) force microscopy, Phys. Rev. B 64 (2001) 193411.
[48] B. Anczykowski, B. Gotsman, H. Fuchs, J. P. Cleveland, V. B. Elings, How to measure energy dissipation in dynamic mode atomic force microscopy, Appl. Surf. Sci. 140 (1999) 376.
[49] A.F. Payam, M. Fathipour, Study of the tip mass and interaction force effects on the frequency response and mode shapes of the AFM cantilever, Int. J. Adv. Manuf. Technol. 65 (2013) 957-966.